SCIENTIFIC REPORTS

OPEN

SUBJECT AREAS:
BATTERIES
POROUS MATERIALS
NANOPARTICLES
SYNTHESIS AND PROCESSING

Received
3 January 2013

Accepted
7 March 2013

Published
28 March 2013

Correspondence and requests for materials should be addressed to Q.W.C. (cqw@ustc.edu.cn)

Hollow Porous SiO_2 Nanocubes Towards High-performance Anodes for Lithium-ion Batteries

Nan Yan, Fang Wang, Hao Zhong, Yan Li, Yu Wang, Lin Hu & Qianwang Chen

Hefei National Laboratory for Physical Sciences at Microscale, Department of Materials Science & Engineering, and Department of Chemistry, University of Science and Technology of China, Hefei 230026, P. R. China.

The high theoretical capacity and low discharge potential of silicon have attracted much attention on Si-based anodes. Herein, hollow porous SiO_2 nanocubes have been prepared via a two-step hard-template process and evaluated as electrode materials for lithium-ion batteries. The hollow porous SiO_2 nanocubes exhibited a reversible capacity of 919 $mAhg^{-1}$ over 30 cycles. The reasonable property could be attributed to the unique hollow nanostructure with large volume interior and numerous crevices in the shell, which could accommodate the volume change and alleviate the structural strain during Li ions' insertion and extraction, as well as allow rapid access of Li ions during charge/discharge cycling. It is found that the formation of irreversible or reversible lithium silicates in the anodes determines the capacity of a deep-cycle battery, fast transportation of Li ions in hollow porous SiO_2 nanocubes is beneficial to the formation of Li_2O and Si, contributing to the high reversible capacity.

Lithium-ion batteries (LIBs) are the dominant power source for a wide range of portable electronic devices due to their high energy density, long lifespan and environment benignity[1,2]. Even though the property of LIBs has been already been considerably enhanced in recent years, further improvement of both their energy density and power density is still attracting much attention[3,4]. As the commercial LIBs anode material, graphite has a relatively low theoretical discharge capacity of 372 $mAhg^{-1}$. Therefore, the preparation of different anode materials with high capacity has been explored, such as alloys, metal oxides, and metal sulfides[5]. Silicon is known to have the highest theoretical specific capacity (4200 $mAhg^{-1}$) and considered to be an optimal anode material for the next generation LIBs[6–11]. However, the drastic volume variation (around 300%) during repeated insertion and extraction of lithium ions leads to its remarkable capacity fading[12]. Some novel silicon-based nanomaterials such as nanowire[6,7], hollow nanoparticle[8], nanotube[9], Si-C nanocomposite[10] and york-shell nanoparticle[11] have shown improved cycling performance, however, they are usually prepared by a multi-step and advanced fabrication process, making the product costly. As an alternative, silica (SiO_2) has been considered to be the anode material of LIBs because of the analogous advantage of storing a large quantity of lithium and low discharge potentials[13]. Besides, SiO_2 is one of the most abundant materials on Earth and the major constituent of sand and therefore, the cost is cheaper than other metal-based materials. In the past decades, silica is not generally considered to be electrochemically active for lithium storage until Gao et al. reported that commercial SiO_2 nanoparticles could react with Li between 0.0 and 1.0 V (vs. Li/Li^+) with a reversible capacity of 400 $mAhg^{-1}$ [14]. After that, some investigations on SiO_2 materials with different structures have been reported for application as LIBs anodes, such as film, carbon-coated nanoparticles, hollow nanospheres and so on[15–19]. Although the theoretical specific capacity of SiO_2 was calculated to be 1965 mAh/g, the electrochemical performance was not obviously improved for the reasons of volume expansion effect and generating irreversible lithium silicate particles via the electrochemical reaction during cycling[16]. For example, the carbon-coated SiO_2 nanoparticles showed a discharge capacity of 500 $mAhg^{-1}$ after the 50th cycle at a 50 mAg^{-1} current density[17]. Nakashima's group have synthesized hollow silica nanospheres with uniform size of about 30 nm, and the hollow nanospheres exhibited a reversible discharge capacity of 336 $mAhg^{-1}$ after the 500th cycle at 1C current density[18]. Thus, the capacity of silica anode material has a large potential to be enhanced, which relies on the precise designing of nanostructures to achieve this unique functionality.

Hollow porous nanostructure materials are of great interest in many current emerging areas of technology. With their unique structures, they bring great advantages such as well-defined morphology, uniform size, low density, large surface area[20–22]. Thus, hollow nanoparticles are used in catalysis, energy conversion, adsorption,

drug deliver and gas sensor[23–27]. When used as electrode materials for LIBs, hollow porous nanoparticles could reduce lithium diffusion path length to enhance the electrochemical properties such as rate performance and cyclability. In addition, the hollow interior can provide extra free space for alleviating the structural strain and accommodating the large volume variation during the repeated reversible reaction between Li^+ ions and electrode materials, especially metal oxide and Si-based materials[28]. Therefore, the hollow porous nanostructures of some materials involving carbon, metal oxide, silicon, were synthesized for the application of LIBs[29–32]. Generally, nanomaterials with hollow porous structure exhibit a nanoscale pore size distribution in the shell. These mesopores shorten electrolyte diffusion path length into the interior of hollow structure, while they could be blocked due to the volumetric expansion if the pore size is smaller, resulting in capacity fading during cycling. Some previous researches have demonstrated that increased pore size can improve electrochemical property, being displayed in mesoporous single-crystal Co_3O_4 nano-needles and cobalt oxide nanowall arrays[33,34]. Our research group has also reported that Co_3O_4 porous nanocages and foamlike porous spinel nanopaticles with wide pore diameter distribution exhibited excellent Li-ion storage capability[35–37]. Namely, it is necessary to modify the surface of electrode material and make sure that electrolyte can pass through the channel. According to the studies cited above, designing and preparing hollow SiO_2 nanoparticles with porous shells as anode materials can improve the discharge capacity because it not only can let more Li^+ flux across the interface but also accommodate the large volume variations during cycling. Simultaneously, the modified porous shells could maintain the reversible movement of Li^+ ions between inside and outside of the hollow nanoparticles even though inactive lithium silicates generated. Herein, we report on the preparation of hollow porous SiO_2 nanocubes (HPSNCs) with numerous crevices in the shell via a two-step hard-template way and their potential applications as anode materials for LIBs.

Results

Fig. 1 schematically illustrates the procedure of generating hollow porous SiO_2 nanocubes (HPSNCs). Firstly, uniform $Co_3[Co(CN)_6]_2$ nanoparticles were coated with SiO_2 during the sol-gel process of tetraethyl orthosilicate (TEOS), producing $Co_3[Co(CN)_6]_2@SiO_2$ nanoparticles with a typical core/shell structure. The next step was the calcination of the core/shell nanoparticles, $Co_3[Co(CN)_6]_2$ cores were in situ converted to large amount of monodisperse well-crystalline Co_3O_4 nanocrystals owing to Ostwald ripening effect during the process of thermal decomposition[38]. Meanwhile, the porous SiO_2 shell could maintain the previous shape due to its thermal stability. We have evaluated the catalytic performance of $Co_3O_4@SiO_2$ nanorattles in the previous report[39]. Herein, the generated $Co_3O_4@SiO_2$ nanorattles were etched by hydrochloric acid solution and the Co_3O_4 could be removed easily. After the two-step hard-template way, the HPSNCs were prepared. The reasons of using such a two-step process are as following: On the one hand, the $Co_3[Co(CN)_6]_2$ nanoparticles as templates are hard to remove only by acid etching. On the other hand, during the process of calcination and acid etching, the gaseous products generated inside of silica nanocubes can escape as well as the hot acid solution can enter in the interior, which is helpful to form and expand the crevices on the surface of SiO_2 nanocubes. The crevices serve as channels for electrolyte to penetrate into interior of SiO_2 nanocubes, which could reduce lithium diffusion path length.

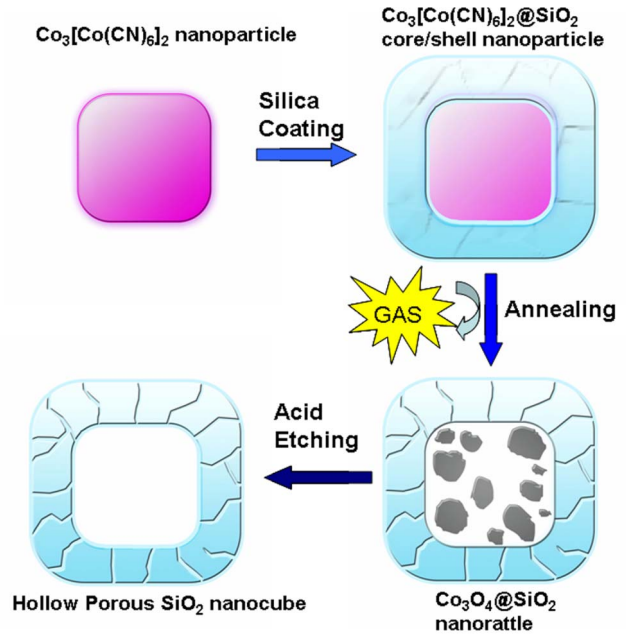

Figure 1 | Schematic illustration of the formation process of a hollow porous SiO_2 nanocube.

The crystallographic structure of the material was analyzed by X-ray diffraction (XRD), shown in Fig. 2(a). The red line reveals the XRD pattern of $Co_3O_4@SiO_2$ nanorattles, while the black line indicates the formation of HPSNCs. Compared the two patterns, it can be seen that there are obvious diffraction peaks in the pattern of $Co_3O_4@SiO_2$ nanorattles, corresponding well to spinel Co_3O_4 (JCPDS card no. 42–1467, space group: Fd3m, lattice constant $\alpha = 8.08$ Å). Moreover, there is a weak broadening band between 20° and 25°, which indicates the presence of amorphous SiO_2. After being acid etched, the peaks of spinel Co_3O_4 disappear, while the broad diffraction band is still present. The result of XRD analysis indicates the complete removing of Co_3O_4 and remaining of amorphous SiO_2.

The FT-IR spectra, shown in Fig. S1 (See Supplementary information online), also describe the samples owning amorphous SiO_2, such as $Co_3[Co(CN)_6]_2@SiO_2$ nanoparticles, $Co_3O_4@SiO_2$ nanorattles and HPSNCs, all show a peak at 1071 cm^{-1} which can be attributed to superimposed asymmetric Si–O–Si stretching bands as well as the symmetric Si–O–Si stretching bands around 800 cm^{-1}. In addition, two strong peaks at 670 and 574 cm^{-1} in the spectrum of $Co_3O_4@SiO_2$ nanorattles and Co_3O_4 nanoparticles are related with a cobalt−oxygen bond[38]. The absence of the two peaks in the spectrum of HPSNCs also proves that Co_3O_4 cores were removed, corresponding to XRD results.

The morphology of the samples was shown in Fig. S2, $Co_3[Co(CN)_6]_2$ nanoparticles are large and uniform in both size and shape. The morphology of $Co_3[Co(CN)_6]_2$ nanoparticles can be described as truncated nanocubes, thus producing the cube shape of coated SiO_2 shells. After the hydrolysis reaction of tetraethyl orthosilicate, the smooth surface of nanoparticles became rough, which indicates that amorphous SiO_2 was coated on the $Co_3[Co(CN)_6]_2$ nanoparticles (See Fig. S3). Moreover, as a result of the sol-gel process of tetraethyl orthosilicate, there are many crevices in the amorphous silica shell. Thanks to the thermal stability of SiO_2 shell, the appearance and shape of $Co_3O_4@SiO_2$ nanorattles have not been changed after annealing at 550°C, which can be seen from Fig. S4. But the crevices in amorphous SiO_2 shell enlarged due to the gaseous products escaping from the interior of nanoparticles. As shown in Fig. 2(b), the as-prepared HPSNCs display excellent dispersibility and uniform shape with an average diameter of 150 nm. From the magnified SEM image shown in Fig. 2(c), the crevices on the surface of SiO_2 nanocubes can be observed. Simultaneously, the hollow interior can be seen through the broken shell of some SiO_2 nanocubes. These SEM images reveal the presence of hollow SiO_2 nanocubes with crevice shells.

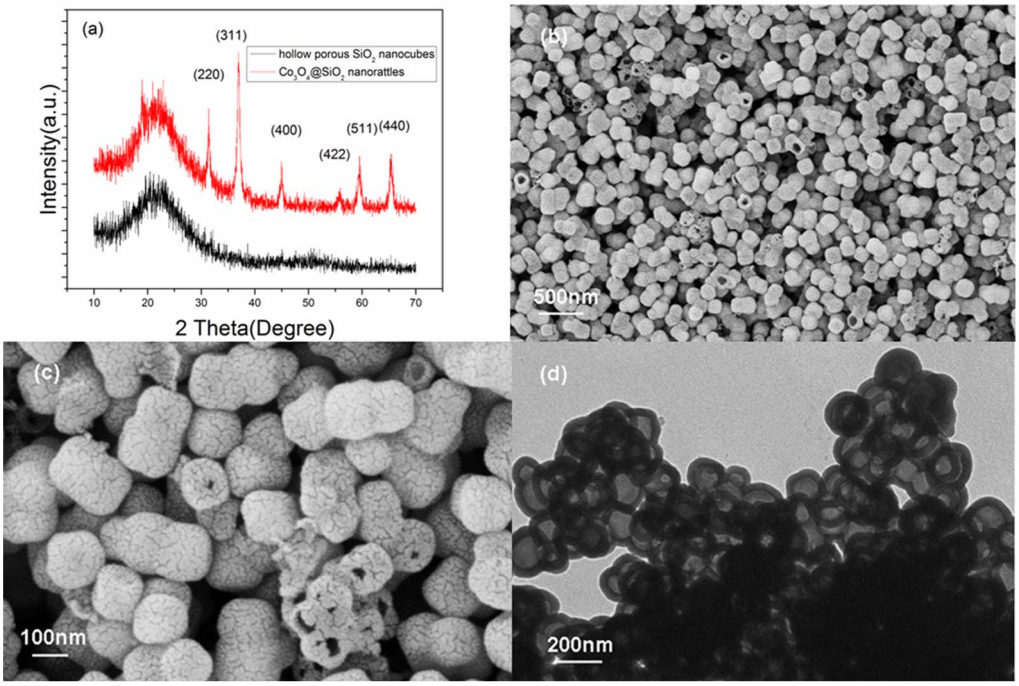

Figure 2 | (a) XRD patterns of Co_3O_4@SiO_2 nanorattles and hollow porous SiO_2 nanocubes, (b) and (c) SEM images of hollow porous SiO_2 nanocubes, (d) TEM image of hollow porous SiO_2 nanocubes.

TEM images also reveal that the solid structure of $Co_3[Co(CN)_6]_2$ nanoparticles (Fig. S5) were changed into core/shell structures (Fig. S6) after SiO_2 coating. When annealed at 550°C for 1 h, the Co_3O_4@SiO_2 nanoparticles demonstrate a typical rattle-type structure (Fig. S7). A TEM image shown in Fig. 2(d) reveals the hollow nature of SiO_2 nanocubes, and the thickness of the silica shell is 20 nm. The N_2 absorption−desorption isotherms at 77 K are shown in Fig. S8 and characteristic of a type IV with type H3 hysteresis loop, which confirms the porous structure of HPSNCs. The specific surface area calculated with the BET model is 51.13 m^2g^{-1}. A wide bimodal-pore size distribution with detectable sizes of 5.5 and 10 nm can be clearly distinguished from the pore size distribution curve (Fig. S9), which is corresponded well with the irregular distribution of crevices on the surface of HPSNCs.

To investigate the electrochemical performance of HPSNCs, two-electrode 2032 coin cells with HPSNCs anodes were fabricated with Li metal as the counter electrode. The electrochemical performance of HPSNCs was firstly evaluated by cyclic voltammetry (CV) in the 0–3.0 V voltage window (Fig. 3(a)). There are obviously two reduction peaks in the potential of 1.3 V and 0.55 V, which appear only in the first cycle. It is reasonable to assume that the peak at the higher potential is due to the irreversible reactions between the electrode and electrolyte[29]. The peak at 0.55 V is associated with the electrolyte decomposition and the formation of the solid electrolyte interface (SEI) layer[15–19]. Both would contribute to the large irreversible capacity of the first discharge process. The discharge and charge voltage profiles of different cycles shown in Fig. 3(b) are in good agreement with the CV measurements. A plateau at 0.5 V can be observed only in the first discharge voltage profile, corresponding to the peaks in CV curves. The discharge and charge capacities of the 1st cycle are 3084 and 1457 $mAhg^{-1}$, respectively, with a low initial Coulombic efficiency of 47%. The discharge capacity of the 2nd cycle is 1807 $mAhg^{-1}$. Such a large irreversible capacity (1277 $mAhg^{-1}$) can be attributed to the formation of SEI layer and irreversible electrochemical reactions between lithium ions and SiO_2, for instance, the generation of lithium salt and some of Li remained in the conducting agent[16,17]. In the following discharge/charge process, the voltage profiles show a similar shape and the electrochemical performance of HPSNCs becomes stable.

The curves of capacity versus cycle number at a current density of 100 mAg^{-1} are shown in Fig. 3(c). From the profile, it can be found that the HPSNCs exhibited a reasonable cycle performance. Despite

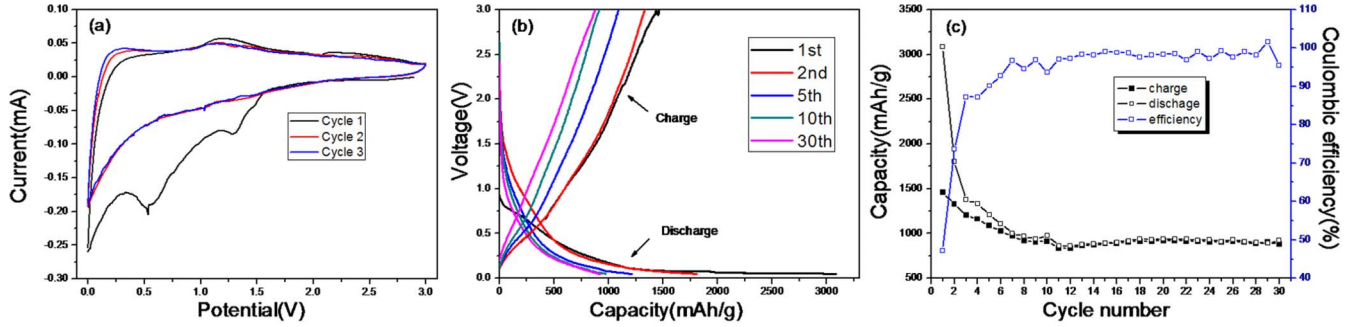

Figure 3 | (a) Cyclic voltammetry of hollow porous SiO_2 nanocubes between 3 and 0 V at a scan rate of 0.1 mVs^{-1}, (b) Galvanostatic discharge/charge voltage profiles of hollow porous SiO_2 nanocubes at a rate of 100 mAg^{-1}, (c) Discharge capacities versus cycle number of hollow porous SiO_2 nanocubes at the current density of 100 mAg^{-1} between 3 and 0 V.

the capacity decayed in the initial five cycles, even after 30 cycles, the discharge capacity can retain a large value of 919 $mAhg^{-1}$. To our knowledge, this remarkable capacity is larger than all of the previous reports of SiO_2-based material anode, such as SiO_2 film[15], nano-SiO_2 in hard carbon[16], carbon-coated SiO_2 nanoparticles[17], hollow SiO_2 nanospheres[18] and milled quartz[19]. In addition, the initial Coulombic efficiency of 47% recovered to 73% in the second cycle, and maintained almost 95% in the subsequent cycles. Furthermore, the HPSNCs also demonstrated outstanding performance at a large current density. As shown in Fig. S10, the initial discharge capacity is 1269 $mAhg^{-1}$ and remains 377 $mAhg^{-1}$ after 25 cycles at a current density of 500 mAg^{-1}, which is also better than the commercial graphite anode (Theoretical capacity of 372 $mAhg^{-1}$). The rate discharge capacity of the anode material was evaluated and shown in Fig. S11. From the profiles, the HPSNCs showed a stable cycling behavior at different current densities. The discharge capacity decreased when the hollow silica nanocubes were cycled at a high current rate of 2400 mAg^{-1}, while resumed to 1021 $mAhg^{-1}$ at a rate of 100 mAg^{-1}. The reasonable electrochemical performance of HPSNCs can be partially attributed to the advantages of hollow porous structures, such as greatly enhancing diffusion kinetics and buffering the volumetric change[28]. Wang et al. have synthesized a series of multi-shelled Co_3O_4 hollow spheres, including single-, double-, and triple-shelled structures, and compared their lithium storage capacities. The experiment results revealed the importance of a suitable void space for electrochemical performance[40]. In our research, the sufficient inner space (diameter of 100 nm) and thick shell (thickness of 20 nm) of HPSNCs can accommodate the volume change and alleviate the structural strain. Moreover, the numerous crevices in the shell of HPSNCs can avoid being unblocked due to the irregular distribution and large pore size, hence allowing the electrolyte passing through during cycling. The change of structure during the discharge/charge process is shown in Fig. 4. Owing to the unique hollow porous construction, the HPSNCs could maintain the original shape. In addition, the shell was thickened from 20 nm to 45 nm due to the generation of SEI film and Li-Si alloy after discharge. Then, the change of thickness of SiO_2 shell repeated in the next cycles. The TEM images of each type of nanoparticles under the model diagrams reveal the structure transformation of SiO_2 nanocubes. The smooth corners can adapt to the large stress during volume expansion, which is better than standard cubes. According to the SEM image of the mixture on the electrode after 30 cycles (Fig. S12), the truncated nanocubes can be observed clearly, which proved the structural stability of the silica nanocubes. As a result, the discharge capacity and cycle stability are enhanced. This is the reason why the electrochemical performance of the HPSNCs is better than the reported hollow SiO_2 nanospheres with a void space diameter of 13.9 nm and wall thickness of 5.8 nm, exhibiting a low reversible discharge capacity of 472 $mAhg^{-1}$ after 2 cycles and further decreasing in the following cycles[18]. It is suggested that the small size of hollow nanoparticles can enhance the cycle stability for the minor volume expansion effect, but the relative thick SEI film generated in the surface of nanoparticle may also decrease the reversible capacity[9].

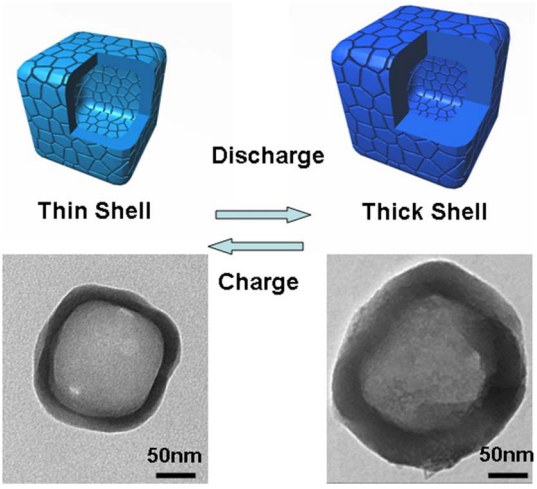

Figure 4 | Schematic illustration for the structure change of hollow porous SiO_2 nanocubes during the discharge/charge process. The TEM images reveal the structure of a single SiO_2 nanocube before and after discharge.

Discussion

The electrochemical reaction mechanism of SiO_2 with lithium ions has been examined by Fu's group for the first time[15]. XPS measurement was carried out to detect the composition of the SiO_2 thin film of the as-deposited, the discharging 0.01 V and charging to 3.0 V. The results showed that the peak position of O 1s shifted toward low energy after discharging to 0.01 V and returned to the high energy when further charging to 3.0 V, while there was no measurable chemical shift for binding energy of Si 2p XPS spectrum. Combined with the HR-TEM and SAED data, the mechanism was expressed as follows:

$$5SiO_2 + 4Li^+ + 4e \leftrightarrow 2Li_2Si_2O_5 + Si \quad (1a)$$

$$Si + xLi^+ + xe \leftrightarrow Li_xSi \quad (1b)$$

The two reactions are all reversible. However, Guo et al. have suggested another mechanism[16]. They studied the chemical state of Si and O atoms using XPS measurement. In their research, the O 1s peak of the sample red–shifted after discharging to 0 V and did not shift back even after recharging to 3.0 V. Simultaneously, Si 2p peak exhibited a remarkable broadening, indicating that the chemical state of Si is complicated rather than a single one. Thus another mechanism was proposed as follows:

$$SiO_2 + 4Li^+ + 4e \rightarrow 2Li_2O + Si \quad (2a)$$

$$2SiO_2 + 4Li^+ + 4e \rightarrow Li_4SiO_4 + Si \quad (2b)$$

$$Si + xLi^+ + xe \leftrightarrow Li_xSi \quad (2c)$$

The reaction of 2a and 2b are irreversible and parallel while the reaction 2c is responsible for the reversible capacity. By comparing the two mechanisms, it can be summed that three types of reaction exist between silica and Li ions. According to these reaction equations, the theoretical capacity of SiO_2 has been calculated based on the number of transfer electrons and shown in Table 1 (supposing that $Li_{22}Si_5$ is the end product of discharge). The molar ratio of SiO_2 and Li ions in the reaction equations is also displayed in Table 1, which reveals that the theoretical capacity of SiO_2 increases with the reduction of the amount of silica. Namely, the reaction generated Li_2O and Si shows the largest reversible capacity of 1961 $mAhg^{-1}$. This result is easy to understand because the SiO_2 is completely converted to Si and stored Li ions in the next process, while inactive lithium silicate is generated via other reactions.

In our work, XPS measurement was also employed to investigate the chemical composition of HPSNCs in different cycle processes. Fig. 5(a) shows the spectra of Si 2p of different kinds of samples. It clearly indicated that the peak centers at 103.27 eV assigned to the amorphous SiO_2 and shifts to 103.04 eV after discharging to 0 V, which describes the formation of Li_4SiO_4 and pure Si[16]. Then the peak shifts back to 103.25 eV. Such a phenomenon of approximate recovery is different from the mentioned references, which suggests complex irreversible and reversible reactions of Si element involved, for instance, the reaction 1a, 2a and 2b. The spectra of O 1s was shown in Fig. 5(b). It can be seen that the peak of as-prepared HPSNCs at 532.71 eV shifts toward to a low energy of 531.93 eV,

Table 1 | The theoretical capacities and the molar ratios of SiO_2 and Li ions in different mechanisms

	Reaction equations	The molar ratio of SiO_2 and Li ions	Theoretical initial capacity of SiO_2	Theoretical reversible capacity of SiO_2
Mechanism 1 Ref. 15	$5SiO_2+4Li^+ + 4e \leftrightarrow 2Li_2Si_2O_5 + Si$ $5Si + 22Li^+ + 22e \leftrightarrow Li_{22}Si_5$	5 : 4	749 $mAhg^{-1}$	749 $mAhg^{-1}$
Mechanism 2 Ref. 16	$2SiO_2 + 4Li^+ + 4e \rightarrow Li_4SiO_4 + Si$ $5Si + 22Li^+ + 22e \leftrightarrow Li_{22}Si_5$	1 : 2	1872 $mAhg^{-1}$	980 $mAhg^{-1}$
Mechanism 2 Ref. 16	$SiO_2 + 4Li^+ + 4e \rightarrow 2Li_2O + Si$ $5Si + 22Li^+ + 22e \leftrightarrow Li_{22}Si_5$	1 : 4	3744 $mAhg^{-1}$	1961 $mAhg^{-1}$

closed to the $Li_2Si_2O_5$[13], when discharged to 0 V. After further charging to 3 V, the peak moves to the energy of 532.13 eV, which indicates the decomposition of $Li_2Si_2O_5$, with an irreversible change due to the generation of Li_4SiO_4 and Li_2O. Therefore, it is suggested that the reversible reaction of $Li_2Si_2O_5$ (reaction 1a) and the irreversible reaction of both Li_2O (reaction 2a) and Li_4SiO_4 (reaction 2b) are coexistence in the electrochemical reaction between silica and Li ions. Recently, Sohn's group has also demonstrated the similar mechanism when using quartz as anode materials[19]. The large reserved capacity depends on the formation of Li_2O and Si, and a plausible hypothesis has been proposed that small SiO_2 nanoparticles preferred to form Li_2O and Si[16]. According to the discussed mechanism, the way to improve cycle capacity is to increase the yield of reaction 2a, which depends on Li ions transportation. As for HPSNCs, the hollow porous structure and numerous crevices can ensure rapid access of Li ions, making the reaction mainly proceed via reaction 2a, forming Li_2O and Si as much as possible. The generated irreversible lithium salts could remain in the shell of nanocubes as framework, which could enhance the structure stability and accommodated volume expansion. Therefore, HPSNCs are better than Si electrodes typically suffering from poor capacity retention related to its large expansion/contraction during cycling. Thus, this is also one of the reasons for the large reversible capacity of HPSNCs.

In summary, hollow porous SiO_2 nanocubes (HPSNCs) were generated by a two-step hard-template process and shown a discharge capacity of 919 $mAhg^{-1}$ after 30 cycles as anode materials for Li-ion batteries. It is considered that the unique hollow porous nanostructure with numerous crevices in the shell can adapt to the volume expansion during cycling. Moreover, the structure could also reduce the diffusion path length of lithium ions and supply enough Li ions to react with SiO_2, which is necessary for increasing the formation ratio of Li_2O and Si and improving the performance of SiO_2 electrodes.

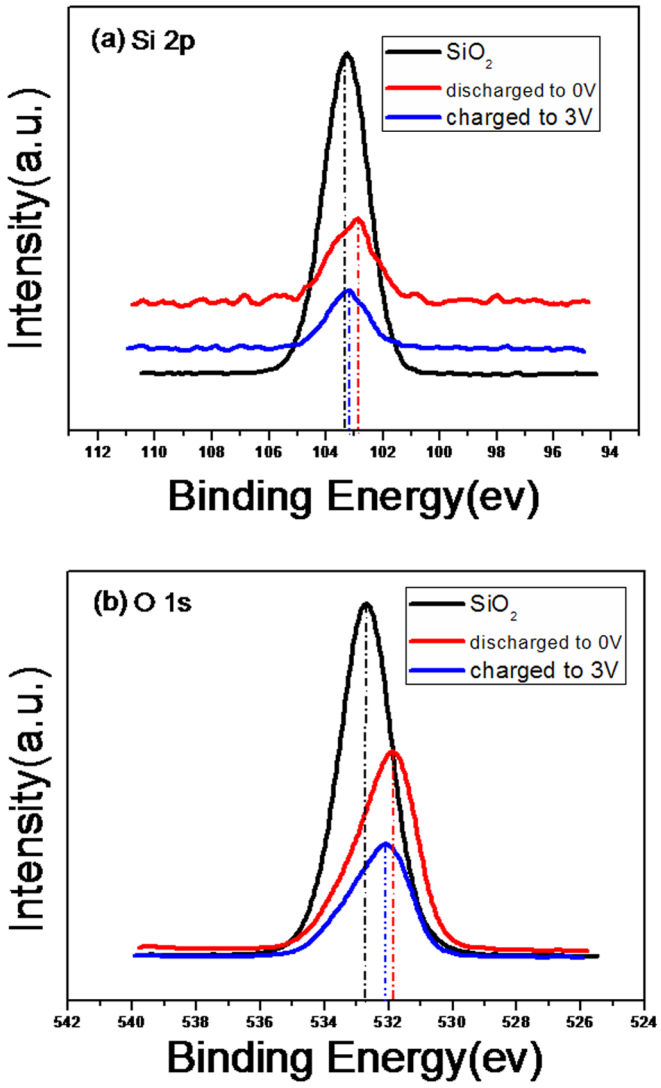

Figure 5 | (a) Si 2p and (b) O 1s XPS spectra for hollow porous SiO2 nanocubes of as-prepared, discharged to 0 V and charged to 3 V, respectively.

Methods

Synthesis. All chemicals are of analytical grade and used without purification. The typical synthetic experiments were conducted in the following steps: The $Co_3[Co(CN)_6]_2$ nanoparticles were synthesized following the previous reports of our group[41]. 60 mg of the as-prepared $Co_3[Co(CN)_6]_2$ nanoparticles and 0.35 mL tetraethyl orthosilicate (TEOS) were dispersed in 30 mL ethanol. After intensely sonicated for 10 minutes, 6 mL concentrated ammonia solution (28 wt%) was added dropwise in 5 minutes. The reaction was allowed to proceed for 4 h at 45°C under continuous mechanical stirring. The resulting $Co_3[Co(CN)_6]_2$@SiO_2 core/shell nanoparticles were centrifuged and washed twice with distilled water, then dried in air at 60°C. The annealing process was performed at 550°C for 1 h in air to obtain Co_3O_4@SiO_2 nanorattles with a heat rate of 10°C min^{-1}. To prepare hollow porous silica nanocubes, 30 mg Co_3O_4@SiO_2 nanorattles was dispersed in 30 mL hydrochloric acid solution (Concentration: 5 $molL^{-1}$) and stirred for 10 minutes. Then the mixed solution was transferred to a Teflon-lined stainless autoclave with a total volume of 50 mL and heated to and maintained at 110°C for 6 h. After the autoclave was cooled naturally to room temperature, white product was collected by centrifuge and washed with distilled water for several times, then air dried at 60°C.

Characterization. The powder X-ray diffraction (XRD) patterns were collected on a Japan Rigaku D/MAX-cA X-ray diffractometer equipped with Cu Ka radiation over the 2θ range of 10–70°. Scanning electron microscopy (SEM) images were performed on a JEOL JSM-6700M scanning electron microscope. Transmission electron microscopy (TEM) images were obtained on a Hitachi H-800 transmission electron microscope, using an accelerating voltage of 200 kV. Specific surface areas were calculated from the results of N_2 physisorption at 77 K (Micromeritics ASAP 2020) by using the BET (Brunauer–Emmet–Teller) and BJH (Barrett–Joyner–Halenda). X-ray Photoelectron Spectrum (XPS) was performed on an ESCALAB 250 X-ray Photoelectron Spectrometer with Al Ka radiation. The FT-IR spectrum was determined using a Magna-IR 750 spectrometer in the range of 500–4000 cm^{-1} with a resolution of 4 cm^{-1}.

Electrochemical measurements. The electrochemical behavior of the as-prepared hollow porous SiO_2 nanocubes was examined using CR2032 coin type cells vs. Li with 1 M LiPF6 in ethylene carbonate and diethyl carbonate (EC:DEC = 1 : 1, v/v) as the electrolyte. The working electrode was fabricated by compressing a mixture of the active materials, conductive material (acetylene black), and binder (polyvinylidene fluoride) in a weight ratio of silica/carbon/PVDF= 5 : 3 : 2 onto a copper foil current collector, then dried at 60°C for 12 h. The loading weight of the mixture on the electrode was 4.6 mg, and the area of electrode is about 1.5386 cm^{-2} (The diameter of

round electrode is 1.4 cm). Therefore, the loading density can be calculated approximately 2.99 mg cm^{-2}. The cells were assembled in an argon-filled glove box (MBraun Labmaster 130). The electrode capacity was measured by a galvanostatic discharge-charge method in the voltage range between 3 V and 0 V at a current density of 100 mAg^{-1} on a battery test system (Neware CT-3008W). Cyclic voltammetry was performed using an electrochemical workstation (CHI 660C) between 0–3 V at a scan rate of 0.1 mVs^{-1}. After cycle performance, the cells were disassembled in the argon-filled glove box (MBraun Labmaster 130) and the working electrodes were taken out, washed with N,N-Dimethylformamide (DMF), then dried in vacuum for 12 h for the following characterizations.

1. Armand, M. & Tarascon, J.-M. Building better batteries. *Nature* **451**, 652–657 (2008).
2. Bruce, P. G., Scrosati, B. & Tarascon, J. M. Nanomaterials for rechargeable lithium batteries. *Angew. Chem. Int. Ed.* **47**, 2930–2946 (2008).
3. Goodenough, J. B. & Kim, Y. Challenges for rechargeable Li batteries. *Chem. Mater.* **22**, 587–603 (2009).
4. Whittingham, M. S. Materials challenges facing electrical energy storage. *MRS Bulletin* **33**, 411–419 (2008).
5. Ji, L. W., Lin, Z., Alcoutlabi, M. & Zhang, X. W. Recent developments in nanostructured anode materials for rechargeable lithium-ion batteries. *Energy Environ. Sci.* **4**, 2682–2699 (2011).
6. Ge, M. Y., Rong, J. P., Fang, X. & Zhou, C. W. Porous doped silicon nanowires for lithium ion battery anode with long cycle life. *Nano Lett.* **12**, 2318–2323 (2012).
7. Chan, C. K. *et al.* High-performance lithium battery anodes using silicon nanowires. *Nature Nanotech.* **3**, 31–35 (2008).
8. Chen, D. Y. *et al.* Reversible lithium-ion storage in siliver-treated nanoscale hollow porous silicon particles. *Angew. Chem. Int. Ed.* **51**, 2409–2413 (2012).
9. Wu, H. *et al.* Stable cycling of double-walled silicon nanotube battery anodes through solid-electrolyte interphase control. *Nat. Nanotech.* **7**, 310–315 (2012).
10. Magasinski, A. *et al.* High-performance lithium-ion anodes using a hierarchical bottom-up approach. *Nature Mater.* **9**, 353–358 (2010).
11. Liu, N. *et al.* A yolk-shell design for stabilized and scalable li-ion battery alloy anodes. *Nano Lett.* **12**, 3315–3321 (2012).
12. Boukamp, B. A., Lesh, G. C. & Huggins, R. A. All-solid lithium electrodes with mixed-conductor matrix. *J. Electrochem. Soc.* **128**, 725–729 (1981).
13. Miyachi, M., Yamamoto, H., Kawai, H., Ohta, T. & Shirakata, M. Analysis of SiO anodes for lithium-ion batteries. *J. Electrochem. Soc.* **152**, 2089–2091 (2005).
14. Gao, B., Sinha, S., Fleming, L. & Zhou, O. Alloy formation in nanostructured silicon. *Adv. Mater.* **13**, 816–819 (2001).
15. Sun, Q., Zhang, B. & Fu, Z. W. Lithium electrochemistry of SiO2 thin film electrodefor lithium-ion batteries. *Applied Surface Science* **254**, 3774–3779 (2008).
16. Guo, B. K. *et al.* Electrochemical reduction of nano-SiO_2 in hard carbon as anode material for lithium ion batteries. *Electrochem. Commun.* **10**, 1876–1878 (2008).
17. Yao, Y., Zhang, J. J., Xue, L. G., Huang, T. & Yu, A. S. Carbon-coated SiO_2 nanoparticles as anode material for lithium ion batteries. *J. Power Sources* **196**, 10240–10243 (2011).
18. Sasidharan, M., Liu, D., Gunawardhana, N. D., Yoshio, M. & Nakashima, K. Synthesis, characterization and application for lithium-ion rechargeable batteries of hollow silica nanospheres. *J. Mater. Chem.* **21**, 13881–13888 (2011).
19. Chang, W. S. *et al.* Quartz (SiO_2): a new energy storage anode material for Li-ion batteries. *Energy Environ. Sci.* **5**, 6895–6899 (2012).
20. Lou, X. W., Archer, L. A. & Yang, Z. C. Hollow Micro-/Nanostructures: Synthesisand Applications. *Adv. Mater.* **20**, 3987–4019 (2008).
21. Zhang, Q., Wang, W. S., Goebl, J. & Yin, Y. D. Self-templated synthesis of hollow nanostructures. *Nano Today* **4**, 494–507 (2009).
22. Hu, J., Chen, M., Fang, X. & Wu, L. Fabrication and application of inorganic hollow spheres. *Chem. Soc. Rev.* **40**, 5472–5491 (2011).
23. Chen, D. & Ye, J. H. Hierarchical WO_3 hollow shells: dendrite, sphere, dumbbell, and their photocatalytic properties. *Adv. Funct. Mater.* **18**, 1922–1928 (2008).
24. Lai, X. Y., Halperta, J. E. & Wang, D. Recent advances in micro-/nano-structured hollow spheres for energy applications: From simple to complex systems. *Energy Environ. Sci.* **5**, 5604–5618 (2012).
25. Wang, B., Wu, H., Yu, L., Xu, R., Lim, T.-T. & (David) Lou, X. W. Template-free Formation of Uniform Urchin-like α-FeOOH Hollow Spheres with Superior Capability for Water Treatment. *Adv. Mater.* **24**, 1111–1116 (2012).
26. Cheng, K. & Sun, S. H. Recent advances in syntheses and therapeutic applications of multifunctional porous hollow nanoparticles. *Nano Today* **5**, 183–196 (2010).
27. Li, X. L., Lou, T. J., Sun, X. M. & Li, Y. D. Highly sensitive WO3 hollow-sphere gas sensors. *Inorg. Chem.* **43**, 5442–5449 (2004).
28. Wang, Z., Zhou, L. & (David) Lou, X. W. Metal oxide hollow nanostructures for lithium-ion batteries. *Adv. Mater.* **24**, 1903–1911 (2012).
29. Tang, K. *et al.* Hollow carbon nanospheres with a high rate capability for lithium-based batteries. *ChemSusChem* **5**, 400–403 (2012).
30. Wang, B., Chen, J. S., Wu, H. B., Wang, Z. Y. & (David) Lou, X. W. Quasiemulsion-templated formation of α-Fe_2O_3 hollow spheres with enhanced lithium storage properties. *J. Am. Chem. Soc.* **133**, 17146–17148 (2011).
31. Wang, Z. & (David) Lou, X. W. TiO_2 nanocages: fast synthesis, interior functionalization and improved lithium storage properties. *Adv. Mater.* **24**, 4124–4129 (2012).
32. Yao, Y. *et al.* Interconnected silicon hollow nanospheres for lithium-ion battery anodes with long cycle life. *Nano Lett.* **11**, 2949–2954 (2011).
33. Lou, X. W., Deng, D., Lee, J. Y. & Archer, L. A. Thermal formation of mesoporous single-crystal Co_3O_4 nano-needles and their lithium storage properties. *J. Mater. Chem.* **18**, 4397–4401 (2008).
34. Zhu, J. X. *et al.* Cobalt oxide nanowall arrays on reduced graphene oxide sheets with controlled phase, grain size, and porosity for Li-ion battery electrodes. *J Phys. Chem. C* **115**, 8400–8406 (2011).
35. Hu, L. *et al.* Fabrication based on the kirkendall effect of Co_3O_4 porous nanocages with extraordinarily high capacity for lithium storage. *Chem. Eur. J.* **18**, 8971–8977 (2012).
36. Hu, L. *et al.* Foamlike porous spinel $Mn_xCo_{3-x}O_4$ material derived from $Mn_3[Co(CN)_6]_2nH_2O$ nanocubes: a highly efficient anode material for lithium batteries. *Chem. Eur. J.* **18**, 15049–15056 (2012).
37. Hu, L. *et al.* $CoMn_2O_4$ Spinel Hierarchical Microspheres Assembled with Porous Nanosheets as Stable Anodes for Lithium-ion Batteries. *Sci. Rep.* **2**, 986. DOI:10.1038/srep00986 (2012).
38. Yan, N. *et al.* Co_3O_4 nanocages for high-performance anode material in lithium-ion batteries. *J. Phys. Chem. C* **116**, 7227–7235 (2012).
39. Yan, N. *et al.* High catalytic activity for CO oxidation of Co_3O_4 nanoparticles in SiO_2 nanocapsules. *J. Mater. Chem. A* **1**, 637–643 (2013).
40. Wang, X. *et al.* Synthesis and lithium storage properties of Co_3O_4 nanosheet-assembled multishelled hollow spheres. *Adv. Funct. Mater.* **20**, 1680–1686 (2010).
41. Hu, L., Zhang, P., Chen, Q. W., Mei, J. Y. & Yan, N. Room-temperature synthesis of Prussian blue analogue $Co_3[Co(CN)_6]_2$ porous nanostructures and their CO_2 storage properties. *RSC Advances* **1**, 1574–1578 (2011).

Acknowledgments

This work was supported by the National Natural Science Foundation (NSFC, U1232211, 21071137) and Foundation of National Science Base (20772188).

Author contributions

Q.W. Chen and N.Y. designed the research, analysed data and wrote the paper. N.Y. and F.W. carried out the electrochemical and physical measurements. Z.H., Y.L., Y.W. and L.H. performed electrochemical measurements and other characterization.

Additional information

Supplementary information accompanies this paper at http://www.nature.com/scientificreports

Competing financial interests: The authors declare no competing financial interests.

How to cite this article: Yan, N. *et al.* Hollow Porous SiO_2 Nanocubes Towards High-performance Anodes for Lithium-ion Batteries. *Sci. Rep.* **3**, 1568; DOI:10.1038/srep01568 (2013).